Hindawi
Journal of Chemistry
Volume 2021, Article ID 6689590, 9 pages
https://doi.org/10.1155/2021/6689590

Research Article

Synthesis of Colloidal Silicon Quantum Dot from Rice Husk Ash

Thu-Huong Le,[1] **Dang Thi Thanh Le**,[1] **and Nguyen Van Tung**[2]

[1]*Faculty of Chemistry and Environment, Thuyloi University, Ha Noi 100000, Vietnam*
[2]*Institute for Technology of Radioactive and Rare Elements, Ha Noi 100000, Vietnam*

Correspondence should be addressed to Thu-Huong Le; lethuhuong@tlu.edu.vn

Received 9 October 2020; Revised 31 January 2021; Accepted 2 February 2021; Published 2 March 2021

Academic Editor: Muhammad J. Habib

This article describes the synthesis procedure of colloidal silicon quantum dot (Si QDs) from rice husk ash. The silicon quantum dots were capped with 1-octadecene by thermal hydrosilylation under argon gas to obtain octadecyl-Si QDs (ODE-Si QDs). The size separation of ODE-Si QDs was examined by the column chromatography method, which used silica gel (40–63 μm) as the stationary phase. Finally, we obtained two fractions of silicon quantum dot, exhibiting blue emission (B-Si QDs) with an average size of 2.5 ± 0.73 nm and red emission (R-Si QDs) with an average size of 5.1 ± 0.68 nm under a UV lamp (365 nm). The PL spectra of B-Si QDs and R-Si QDs samples show maximum peak energy at 410 nm (3.02 eV) and 700 nm (1.77 eV), respectively, while the quantum yield of Si QDs decreases from 5.8 to 34.6% when the average size decreases from 2.5 nm to 5.1 nm. The above results of PL emission spectroscopy and UV-vis absorption show quantum confined effect in Si QDs.

1. Introduction

Colloidal semiconductor silicon nanocrystals or quantum dots of the IV group have received much attention for applications because the size-dependent optical and electronic properties of silicon semiconductor nanocrystals play a key role in various applications such as solar cells, bioimaging, and light-emitting devices [1–3]. Although the quantum yield of silicon quantum dot is lower than the quantum yield of C-dots from biomass, the Si QDs play a key role in various applications such as Li-ion battery, bioimaging, and light-emitting devices [4]. Moreover, silicon is one of the few elements that is nontoxic, earth-abundant, and environmentally friendly. Herein, recent achievements in the synthesis of colloidal Si QDs in terms of controlling the particle size and size distribution and achieving surface modifications make the Si QDs even more promising for the application. Colloidal Si QDs have been synthesized by chemical reduction methods using reducing agents, such as $LiAlH_4$ [5] and sodium naphthalene [6], or by physical methods, such as the thermal processing of hydrogen silsesquioxane [7–9], ion implantation [10], and vacuum evaporation [11]. Unfortunately, these methods have some problems. In the physical and chemical reduction methods, the cost of synthesis is much too high. In chemical reduction methods using reducing agents, the spectrum of color of colloidal Si QDs is obtained with only blue or green color due to defect states on the surface of SiQD. Hence, the investigation of the method of synthesis to provide Si QDs with a minimization of the cost of synthesis, while enabling size control, is of interest. There are some groups reporting the synthesis of Si NCs@SiO_2 by reduction of silica nanoparticle (SiO_2 NPs) using Mg powder [12]. The main advantage of this synthesis method is that it endows easier experimental conditions and more size controllability compared to the previous chemical and physical methods. They report the first synthesis of SiO_2 NPs by a combination of using both the microemulsion of reverse micelles and reduction using Mg powder. These two kinds of synthetic steps were developed independently in the fields of SiO_2 NP and Si NCs synthesis. To investigate how the concentration of water affects the size of SiO_2 NPs in our synthetic procedure, they used different volumes of water (1 ml and 4 ml) without changing the components. The Si NCs sizes obtained by reduction SiO_2 NPs using Mg powder were 20 ± 2.09 nm (for 1 ml water) and 10.66 ± 1.66 nm (designated Si-2, for 4 ml water) [12]. Therefore, they can adjust the size of Si QDs by controlling the size of SiO_2 NPs.

However, most of the studies often use TEOS source and surfactant Brij to synthesize silica [13]. These methods are quite expensive and only stops at the experimental scale, thus limiting the application of silica nanoparticle material. Rice husk ash is one of the richest silica materials about 90% in volume [12], so it is an ideal source of materials to synthesize SiO_2 NPs materials. Besides, now, Vietnam is one of the world leaders in rice production. In 2019, Vietnam's rice output is about 60 million tons/year and the amount of rice husk ash is about 20 million tons/year. Therefore, the investigation of the method of synthesis to provide colloidal Si QDs from rice husk ask with a minimization of the cost of synthesis is still in demand. To respond to this issue, we report the synthesis of silica nanoparticle from rice husk ash; then, Si NCs@SiO_2 was obtained by magnesiothermic reduction silica nanoparticle (SiO_2 NPs) [12]. The chemical etching method was applied to obtain the hydrogen-terminated silicon quantum dot (H-Si QDs), which was functionalized by 1-octadecene at 150°C for 15 hours. The crystal and nanoparticle structure of Si NCs@SiO_2 and colloidal silicon quantum dot were investigated by X-ray diffraction (XRD) spectra, high-resolution transmission electron microscopy (HR-TEM), and selected area electron diffraction (SAED). The optical properties of colloidal silicon quantum dot were estimated by ultraviolet-visible (UV-vis) absorption and photoluminescence spectroscopy (PL).

2. Materials and Methods

2.1. Chemicals and Materials. All chemical reagents, including toluene (anhydrous, 99.8%) and 1-octadecene ($CH_3(CH_2)_{15}CH = CH_2$, 95%), were purchased from Sigma-Andrich. *n*-Hexane (C_6H_{14}, 95%), acetone, and chloroform ($CHCl_3$, 99.7%) were purchased from Dae-Jung (South Korea); magnesium (NH_4OH, 25%) was purchased from Acros organic; and hydrofluoric acid (HF, 48–51%) was purchased from Baker, respectively. Hydrochloric acid (HCl, 36%, $d = 1.18$ g/l), ammonia solution (NH_3, 25%), sodium hydroxide (NaOH), and silica gel (40–63 μm) were purchased from Merck Company of Germany. In our experiment, the rice husk ash (RHA) was obtained from Me village, Bac Giang province, Vietnam.

2.2. Synthesis of Silica Nanoparticles (SiO_2 NPs) from Rice Husk Ash. SiO_2 NPs from RHA were synthesized following the procedure of Sankar et al. [14] with some modifications (Scheme 1). The rice husk ash (RHA) was ground and sifted through a sieve with a hole size of about 0.1 mm to create smoothness powder. 500 ml HCl 1 M was added into 50 g RHA powder and stir overnight to remove residual metal and metal oxide in RHA. Then, RHA powder was collected by vacuum filtration and was put in the furnace at 600°C for 2 hours to remove carbon and some residual organic in the RHA. 45 g RHA powder was stirred with 50 ml of NaOH 3 M at 100°C for 4 hours and then filtered to obtain a transparent solution. The solution HCl 3 M was added to this solution by sonication for 2 hours until pH equals 7. The mixture appeared as a white precipitated powder. The precipitated powder was filtered and washed with distilled water. A white powder was dried at 100°C in the forced air oven for 12 hours. Finally, the obtained product was SiO_2 NPs white powder. The materials and methods section should contain sufficient detail so that all procedures can be repeated. It may be divided into headed subsections if several methods are described.

2.3. Synthesis of Silicon Nanocrystal by Magnesiothermic Reactions. Previously, some groups have synthesized silicon nanocrystal by using magnesiothermic reduction methods [12]. Magnesiothermic reduction offers a straightforward way to convert silica (inexpensive and the most stable source of Si) into elemental silicon while retaining silica particle morphology. Nevertheless, the massive heat release from the exothermic reaction ($Mg + SiO_2 \longrightarrow Si + MgO$, $\Delta H = -586.7$ kJ/mol silica) [15] collapsed the structure of SiO_2 NP and agglomerated silicon crystal into the larger crystal. In this report, the SiO_2 NPs powder (0.60 g, 0.01 mol w.r.t Si content), sodium chloride (6 g), and magnesium powder (0.5 g, 0.22) were mixed and ground together manually to give a grayish brown-colored powder and then heated at 670°C for 15 hours under an argon atmosphere in a quartz tube furnace. The use of NaCl as a heat scavenger during the reduction process ($Mg + SiO_2 \longrightarrow Si + MgO$) prevents the structure from collapsing and aggregation into the larger crystal of the silicon domain. The resulting dark brown-colored powder product was washed by water to remove NaCl and treated with 20 ml hydrochloric acid for 12 hours to remove Mg remaining, Mg_2Si, and MgO. A brown precipitate was obtained by vacuum filtration. And then the solid was washed with distilled water until the washings resulted in a neutral pH (ca. 7). The powder was then washed with ethanol (30 mL) and acetone (3×30 mL) and air-dried to yield oxide-coated Si NCs (Si NCs@SiO_2). Finally, the Si NC@SiO_2 was obtained as a brown powder.

2.4. Synthesis of Colloidal Si QDs. The hydride-terminated silicon quantum dots (H-Si QDs) were synthesized from Si NCs@SiO_2 (0.4 g) powder by using the chemical etching method [15]. Firstly, Si NCs@SiO_2 (1 g) powder was dispersed in a mixture of 50 ml HF (48%) and 20 mL ethanol, which was then sonicated for an additional 6 h at room temperature to remove silicon oxide layers. After completing the etching process, hydride-terminated Si QDs were isolated by extraction with 20 ml of anhydrous toluene and centrifuged using 1200 rpm speed centrifuge for 5 min. After centrifugation, the toluene supernatant was decanted, leaving H-Si QDs. The H-Si QDs were washed with ethanol to remove the remaining HF. Then, 10 ml of 1-octadecene was added to H-Si QDs (Scheme 2). The reaction mixture was degassed by three cycles of evacuation and purging with argon and then heated at 150°C for 15 hours. After the thermal functionalization, the reaction mixture was filtrated to yield a clear, bright yellow. Next, all solvents were removed at 40°C under reduced pressure by using a rotary evaporator. To remove the remaining molecules 1-octadecene, the product was washed three times by precipitation

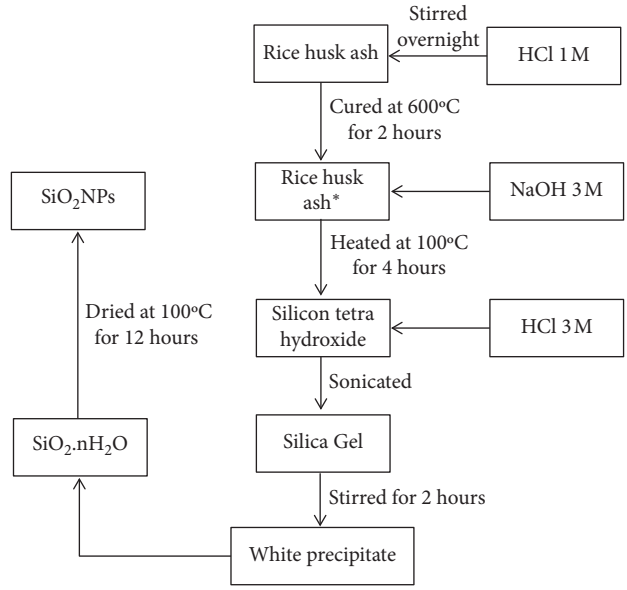

Scheme 1: Synthetic procedure of silica nanoparticles (SiO_2 NPs) from rice husk ash.

with acetone as an antisolvent and dispersed in toluene as a solvent. The product was obtained as a yellow resin after the evaporation of the toluene solvent. The size separation of ODE-Si QDs was examined by the column chromatography method, which used silica gel (40–63 μm) as the stationary phase. The ODE-Si QDs were dissolved in *n*-hexane and introduced into the silica gel column. Size separation was carried out with mixtures of *n*-hexane/chloroform (3/1, v/v) and 100% chloroform. The fractions exhibiting emission of different colors under a UV lamp (365 nm) were collected, and the solvent was removed using a rotary evaporator. Finally, we obtained two fractions of Si QDs, exhibiting blue (B-Si QDs) and red emission (R-Si QDs) under a UV lamp (365 nm) (Scheme 3).

2.5. Characterizations. X-ray diffraction (XRD) spectra of Si NC@SiO_2 powder were obtained using a D8 Advance (Bruker, Germany) and D5005 (Siemens, Germany). FT-IR spectroscopy was performed on a Spectrum 400 (PerkinElmer, USA) to obtain the IR spectra of the Si QDs. The scanning electron microscopy was performed with S-4800 (SEM, Hitachi). High-resolution transmission electron microscopy (HR-TEM) was performed with a JEOL JEM-2100F operated at 200 kV. UV-vis absorption spectra were obtained on an S-3150 UV-vis spectrometer (SCINCO, Korea). Photoluminescence (PL) spectroscopy was performed on an iHR320 Hiroba spectrometer (Hiroba, Japan) light source at the excitation wavelength of 290 nm with a 3 nm slit width and emission monochromators to investigate the quantum yield of B-Si QDs was determined by comparison with quinine sulfate, whose quantum yield is known to be 55% in 0.05 M H_2SO_4. The quantum yield of R-Si QDs was determined by comparison with rhodamine 6 G, whose quantum yield is known to be 94% in ethanol at the excitation wavelength of 480 nm with a 3 nm slit width for both excitation and emission monochromators.

3. Results and Discussion

Figure 1(a) shows the scanning electron microscopy (SEM) image of the SiO_2 NPs sample. The average sizes of the SiO_2 NPs are about 100 nm. The SEM image clearly shows that the particle of the SiO_2 NPs sample is formed, and their size distribution is broad. Moreover, the SEM results of the SiO_2 NPs sample show that many particles aggregate to form a block with a porous structure.

The diffraction pattern of the SiO_2 NPs in Figure 1(b) shows a widened peak of about $2\theta = 20$–25°. These X-ray diffraction (XRD) results indicate that the high percent of SiO_2 NPs were an amorphous phase [14].

Figure 2(a) shows the transmission scanning electron microscopy (TEM) image of Si NC@SiO_2 after magnesiothermic reduction. The TEM image (Figure 2(a)) of Si NC@SiO_2 clearly shows nanoparticles with wide sizes from 2 to 10 nm. However, the crystal structure of Si NC@SiO_2 did not obtain in the TEM image (Figure 2(a)) due to SiO_2 layer, which covers all the surface of silicon nanocrystal. Moreover, X-ray diffraction (XRD) patterns of the Si NC@SiO_2 powder shown in Figure 2(b) exhibit a peak at 2θ of 28.3, 47.3, 56.1, and 69.1, which are well matching with the three characteristic peaks diffracted from the <111>, <220>, <311>, and <400> lattice planes of the diamond cubic silicon crystal [16].

The bonding of 1-octadecene on the surface of Si QDs was confirmed by the FT-IR (Figure 3). For three samples, the alkyl group on surface Si QDs including the asymmetric stretching, symmetric stretching, and in-plane bending or scissoring of the -CH_2- groups were obtained at 2917.1 cm^{-1}, 2847.7 cm^{-1}, and 1372.5 cm^{-1} [17]. The peak at 1466.5 cm^{-1} is attributed to the symmetric bending vibration of a Si-C bond, confirming the formation of the Si-C covalent bond between the Si QDs and octadecyl groups [17].

A purification procedure was necessary to obtain clear TEM images and ensure the samples were free of impurities

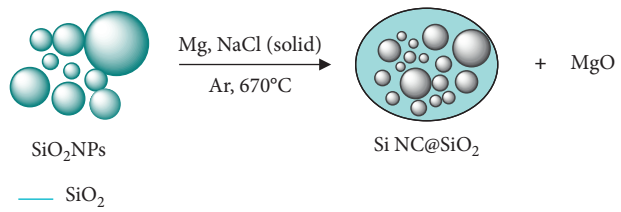

Scheme 2: The synthetic procedure of silicon nanocrystal (Si NC@SiO_2) from silica nanoparticle (SiO_2 NPs).

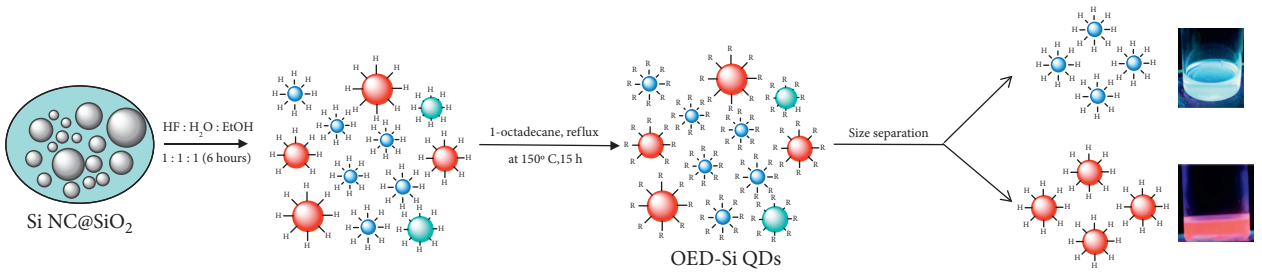

Scheme 3: Synthesis procedure of R-Si QDs and B-Si QDs.

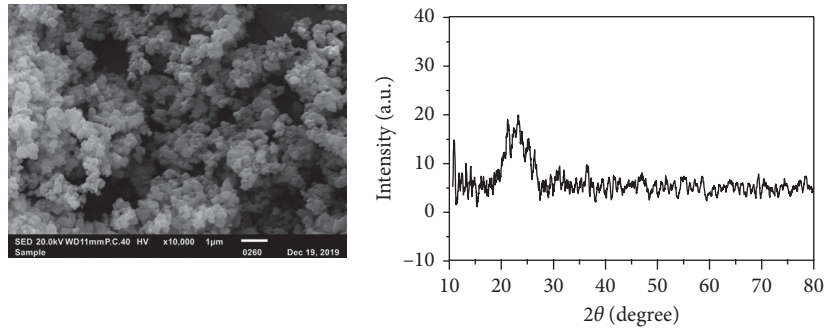

Figure 1: Scanning electron microscopy (SEM) image of SiO_2 NPs (a) and powder X-ray diffraction pattern of SiO_2 NPs (b).

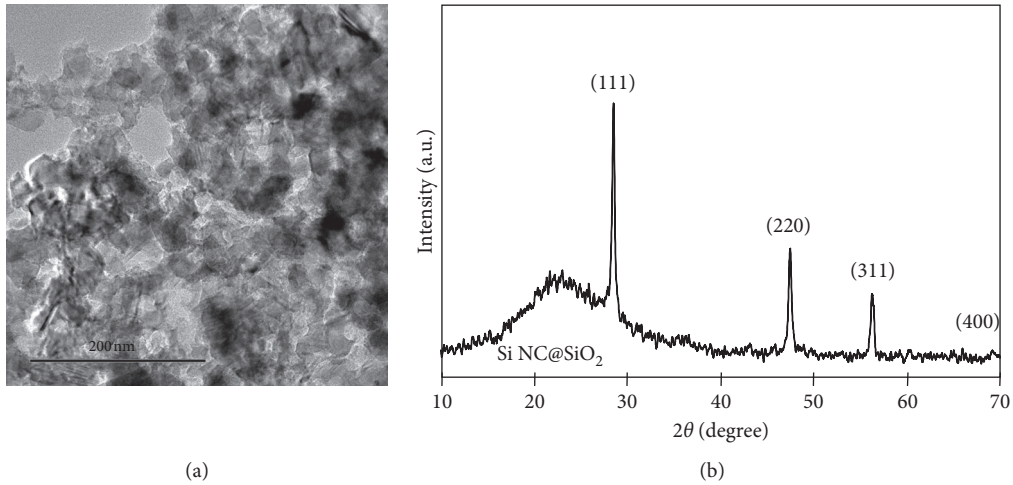

Figure 2: Transmission electron microscopy (TEM) image of Si NC@SiO_2 (a) and powder X-ray diffraction pattern of Si NC@SiO_2 (b).

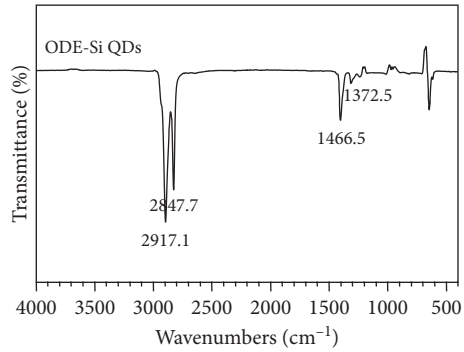

Figure 3: FT-IR spectra of ODE-Si QDs.

before optical characterization. In our synthesis process, the firstly size-selective precipitation method applied, in which the product was washed three times with acetone as an antisolvent and dispersed in toluene, was used for the purification of the ODE-Si QDs to purify residual 1-octadecene and narrow their size distribution; however, this purification process did not completely separate ODE-Si NCs of different sizes, as shown in the TEM image of ODE-Si NCs (Figure 4), and size distribution exhibited two main sizes of about 2.0–3.0 nm and 5.0–6.0 nm. Hence, ODE-Si QDs were purified more by column chromatography. Size separation was carried out with a mixture of *n*-hexane/chloroform (3/1, v/v) and 100% chloroform. Finally, we obtained two fractions of Si QDs, exhibiting blue (B-Si QDs) and red emission (R-Si QD) under a UV lamp (365 nm). Figure 5 shows the transmission scanning electron microscopy (TEM) images of B-Si QDs and R-Si QDs. The TEM images of the two samples clearly show highly spherical dots with average sizes of 2.5 ± 0.73 nm for B-Si QDs and 5.1 ± 0.68 nm for R-Si QDs-5 min samples. Meanwhile, selected area electron diffraction (SAED) shows the d-spacing for (200) Miller indices of 2.7 Å [18]. Therefore, the B-Si QDs and R-Si QDs are the diamond crystal structure.

The optical properties of one Si QDs were investigated by PL emission spectroscopy and UV-vis absorption, as shown in Figure 6. The photoluminescence spectrum was obtained using excitation at 290 nm at room temperature in air, as shown in Figure 6. The photoluminescence spectrum of ODE-Si QDs (black line) showed two intense emission bands at around 410 nm and 700 nm, corresponding to the presence of two size regions in agreement with the TEM results mentioned above (Figure 4). The TEM images of ODE-Si QDs (Figure 4) before size separation by column chromatography show size distribution exhibited two main sizes of about 2.0–3.0 nm and 5.0–6.0 nm. After purification of ODE-Si QDs by column chromatography, we obtained two fractions exhibiting blue (B-Si QDs) and red emission (R-Si QD) under a UV lamp (365 nm) (Scheme 3). The PL spectra of the B-Si QDs sample (blue line) with an average size of 2.5 nm (Figure 6) show maximum peak energy at 410 nm (3.02 eV) while the PL spectra of R-Si QDs sample (red line) average size of 5.1 nm (Figure 6) show maximum peak energy at 700 nm (1.77 eV). The onset of the UV-vis absorption spectrum (Figure 6) was red-shifted from 350 nm (B-Si QDs in hexane) to 400 nm (R-Si QDs in hexane). The above results of PL emission spectroscopy and UV-vis absorption show that it is possible size separation of colloidal Si QDs obtain from rice husk ash by column chromatography. However, the PL spectra and TEM measurements of B-Si QDs and R-Si QDs show maximum peak energy at 410 nm (3.02 eV, blue emission) with average sizes of 2.5 ± 0.73 nm and 700 nm (1.77 eV, red emission) with average sizes of 5.1 ± 0.68 nm, which blue-shift compared with the reports from Yu et al. and Liu et al. [19, 20]. Alternatively, there have been some suggestions that such a blue PL emission of the Si QDs originates from their defect states on the surface [21, 22]. In particular, Dasog and Veinot et al. demonstrated that the blue luminescence can be induced by contaminating red-luminescent Si QD that even follows the quantum confinement effect, by introducing oxygen and nitrogen impurities on the QD surface under oxidative air condition. Dasog et al. concluded that the oxygen and nitrogen impurities probably give surface defect states acting as trap states for the exciton, resulting in the blue luminescence and low quantum yield [21]. Furthermore, Fuzell et al. studied the exciton dynamics of the blue luminescence-directed Si QD from the red-luminescent Si QD, concerning the trap states using ultrafast transient absorption spectroscopy [22]. Hence, in this report, we suggested that the oxygen impurities remain on the surface of B-Si QD and R-Si QD. The existence of oxygen on the surface of Si QD could give surface defect states lead to PL emission of Si QDs shows blue-shift compared with the reports from Yu et al. and Liu et al. [19, 20]. Even though PL emission of B-Si QD and R-Si QD shows blue-shift compared with other reporters [19, 20]. The results of PL emission spectroscopy and UV-vis absorption of R-Si QD still red-shifted compared with B-Si QD, with increasing average sizes of Si QD. Based on these results, we suggest that the emission energy gaps were increased as the size decreased attributed to the quantum confinement effect in Si QD.

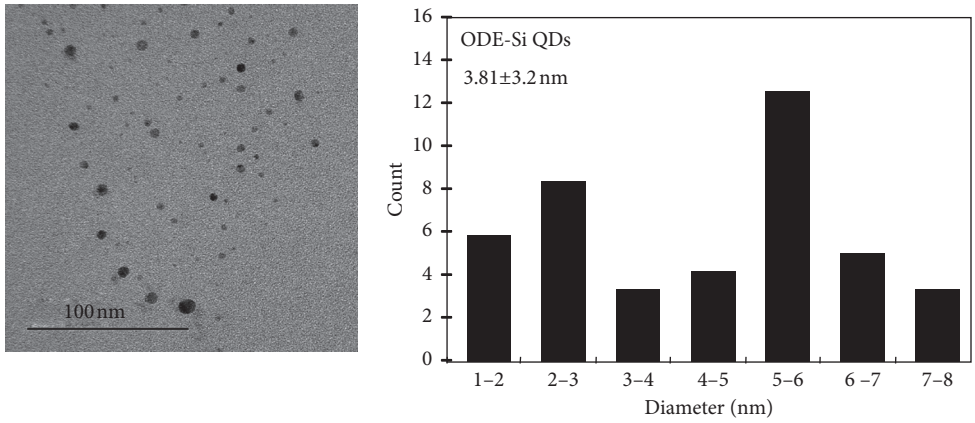

Figure 4: Transmission electron microscopy (FE-TEM) of ODE-Si QDs before size separation by column chromatography.

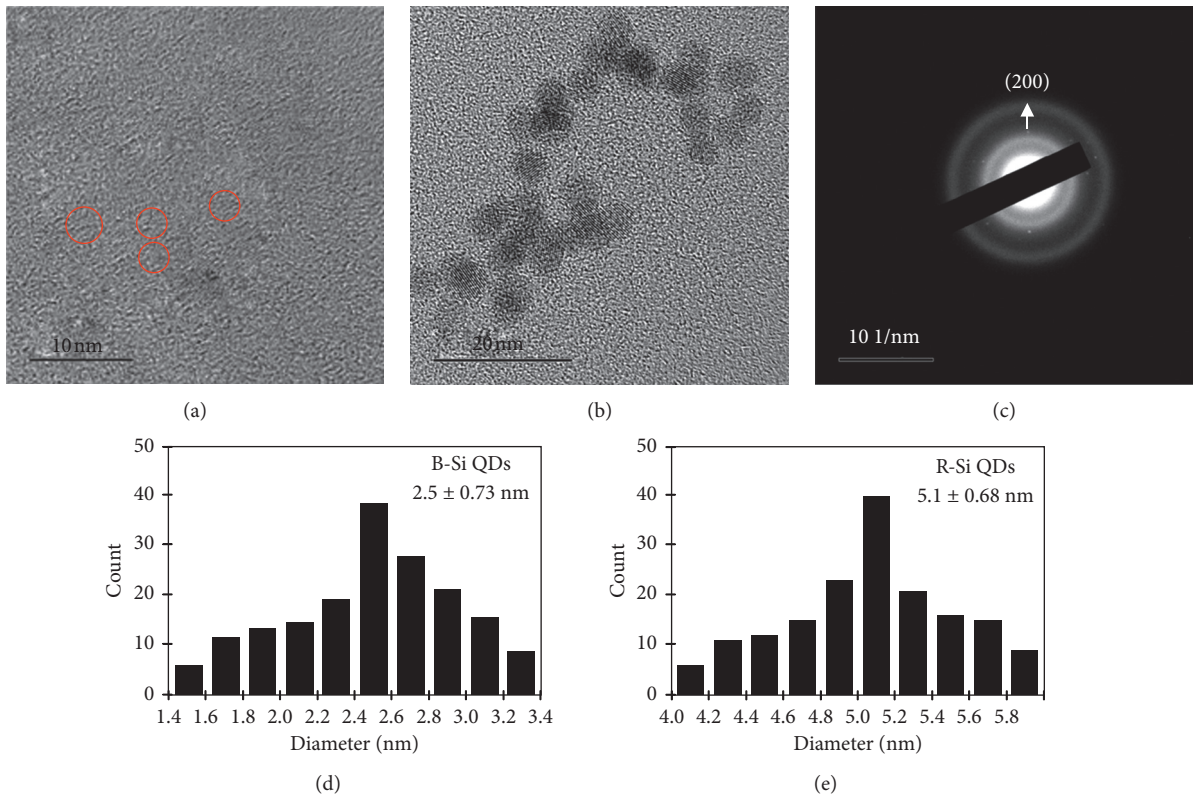

Figure 5: Transmission electron microscopy (FE-TEM): (a-b) selected area electron diffraction (SAED) (c) and size distribution (d-e) of B-Si QDs and R-Si QDs.

The quantum yield of colloidal R-Si QDs and B-Si QDs was determined through the relative approach using the relationship [23]

$$\Phi_s = \Phi_r\left(\frac{I_s}{I_r}\right)\left(\frac{A_r}{A_s}\right)\left(\frac{n_s^2}{n_r^2}\right), \quad (1)$$

where Φ_s and Φ_r are the fluorescent quantum yield of B-Si QD, R-Si QDs, and reference compound; I_s ($I_B = 0.487$, $I_R = 1.61$) and I_r ($I_{\text{quinine sulfate}} = 2.62$, $I_{\text{rhodamine 6G}} = 4.51$) are integrated fluorescence intensity of sample and reference compound; A_s ($A_B = 0.02$, $A_R = 0.042$) and A_r ($A_{\text{quinine sulfate}} = 0.011$, $A_{\text{rhodamine 6G}} = 0.042$) are the absorbance at the excitation wavelength of B-Si QDs (exc = 350 nm), R-Si QDs (exc = 480 nm), and reference compounds, n_s (n-hexane, ns = 1.375), ethanol ($n_r = 1.36$), and n_r (water, $n_r = 1.33$) are the refractive index of the solvent. The absorbance was kept very low and a series of concentrations were examined to avoid any self-absorption or other nonlinear effects. The PL quantum yield

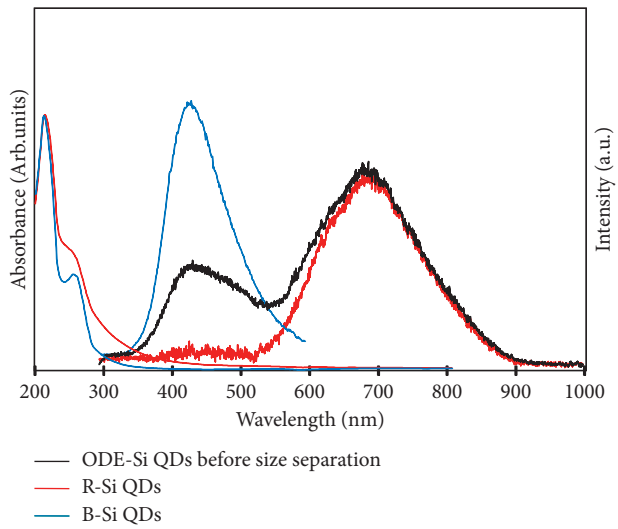

Figure 6: PL emission and UV-vis spectrum of ODE-Si QDs before size separation, R-Si QDs, and B-Si QDs.

(QY) of B-Si QDs (Figure 7(a)) was determined by comparison with quinine sulfate, whose quantum yield is known to be 55% in 0.05 M H_2SO_4 to be 5.8% [23]. The PL quantum yield (QY) of the R-Si QD (Figure 7(b)) was determined by comparison with rhodamine 6G, whose quantum yield is known as 95% in ethanol to be 34.6% [23]. The results of quantum yield and FE-TEM show that the quantum yield of Si QD decreases from 34.6% for R-Si QD with average sizes of 5.1 ± 0.68 nm to 5.8% for B-Si QDs with average sizes of 2.5 ± 0.73 nm. As Ozin's group has reported that the absolute quantum yield and lifetime of photoluminescence of allylbenzene-capped silicon nanocrystal are a function of size [24], the absolute quantum yield was found to monotonically decrease with decreasing nanocrystal size, which implies that non-radiative vibrational and surface defect effect overwhelms spatial confinement effect that favors radiative relaxation [24]. Alternatively, their results showed that Si NC with an average size of ~2.0 nm has a quantum yield of 38%. In our report, the quantum yields of B-Si QDs (average size of $\sim 2.5 \pm 0.73$ nm) and R-Si QDs (5.1 ± 0.68 nm) are 5.8 and 34.6%, respectively, which are lower compared with the reports from Mastronardi et al. [24]. Furthermore, the surface curvature of silicon nanocrystal increases with decreasing particle size, resulting in lower surface group density, it is likely that oxidative species can more easily reach the surface of the small nanoparticle. Therefore, we suggested that the defect surface of Si QD increases with decreasing size would also be expected to contribute to the decrease observed in the quantum yield.

The optical gaps of the B-Si QDs and R-Si QDs were estimated using Tauc plots of $(\alpha h\upsilon)^n$ versus $h\upsilon$ as shown in Figure 8, in which α, h, and υ are the absorption coefficient, Planck constant, and frequency, respectively. The n value was taken as 2 since our Si QDs were assumed to have direct band gap characteristics [18]. The optical gaps of B-Si QDs and R-Si QDs were estimated as 4.4 and 4.2 eV, respectively, as shown in Figure 6 while PL max is approximately 410 (3.02 eV) and 700 nm (1.77 eV). The difference between absorption and emission energies is termed Stokes shift (Table 1). As shown in Table 1, two samples of Si QD (B-Si QDs and R-Si QDs) show size-independence Stokes shift. And the R-Si QDs sample shows a larger Stokes shift than B-Si QDs. There have been some suggestions that the structural relaxation in the excited state of Si QD induces Stokes shift, which varies with the particle size, the degree of surface passivation, and the nature of the passivation species [25, 26]. In particular, Pavesi and Turan demonstrated that the dependence of the Stokes shift from the H-Si NC size qualitatively agrees with the results of the calculations [26]. The Stokes shift decreases when H-Si NC size increases in a small size range from Si_1H_4 to $Si_{10}H_{16}$. The dependence of the Stokes shift from Si NC size qualitatively agrees with the calculations of Zhang et al. [25–27]. Alternatively, Puzder et al. have been determined that, in silicon nanoclusters, the value of Stokes shifts is extremely sensitive to the size, surface structure, and chemistry of the nanocrystal. The Stokes shift results of silicon clusters (size from 1 to 1.8 nm) with Si = O bond to the surface show size independence [27]. As the discussion above, the quantum yields of B-Si QDs (average size of $\sim 2.5 \pm 0.73$ nm) and R-Si QDs (5.1 ± 0.68 nm) are 5.8 and 34.6%, respectively, which are lower compared with the reports from Mastronardi et al. [24]. Therefore, we suggested that the defect surface of Si QD increases with decreasing size would also be expected to contribute to the decrease observed in the quantum yield. Also, the PL spectra of B-Si QDs with the average size of 2.5 ± 0.73 nm show blue emission at 410 nm (3.02 eV). However, Yu et al. reported that alkyl capped Si NC with an average size of 2.5 nm had red emission at 652 nm (1.9 eV) [19]. PL emission of B-Si QDs shows a larger blue-shift compared with the result of Yu et al. reported due to the existence of oxygen on the surface of Si QD while PL spectra of R-Si QDs is maximum peak energy at 700 nm (1.77 eV)

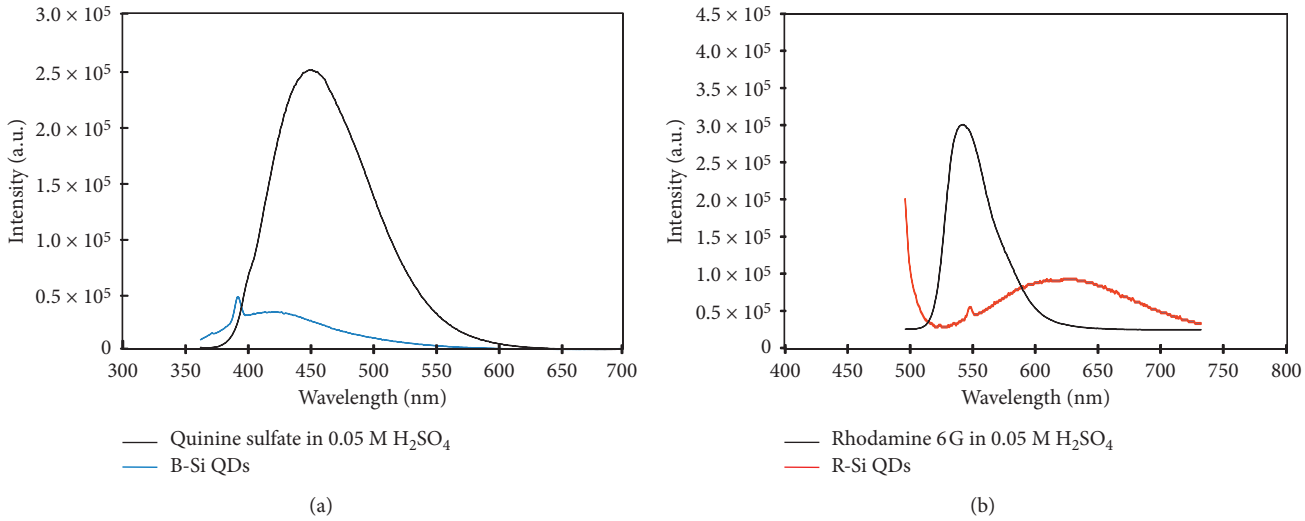

Figure 7: The PL emission of colloidal B-Si QDs (a) and R-Si QDs (b) by comparison with quinine sulfate in 0.05 M H_2SO_4 and rhodamine 6G in ethanol, respectively.

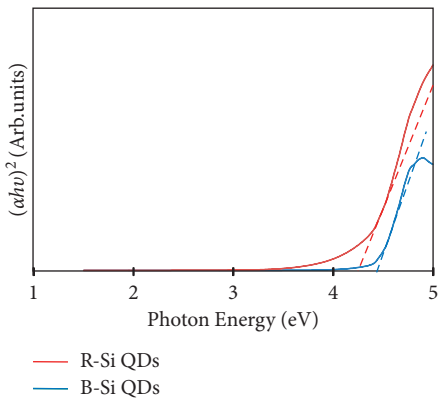

Figure 8: Tauc plot for the R-Si QDs and B-Si QDs.

Table 1: Absorption and emission gaps and Stokes shift.

Sample	Absorption (eV)	Emission (eV)	Stokes shift (eV)
B-Si QDs	4.40	3.02	1.38
R-Si QDs	4.20	1.77	2.43

red emission with the average size of 5.1 ± 0.68 nm which shows a small blue-shift compared with the reports from Yu et al. and Liu et al. [19, 20]. Hence, the difference between absorption gap and emission gap of B-Si QDs (Stokes shift) is smaller than R-Si QDs.

4. Conclusions

In conclusion, colloidal silicon quantum dots (Si QDs) with different size and emission color were synthesized from rice husk ash. Size separation of Si QDs was carried out with a mixture of *n*-hexane/chloroform (3/1, v/v) and 100% chloroform. Finally, we obtained two fractions Si QDs, exhibiting blue emission (B-Si QDs) with average sizes 2.5 ± 0.73 nm and red emission (R-Si QD) with average sizes 5.1 ± 0.68 nm under a UV lamp (365 nm). TEM measurements and photoluminescence results provided evidence of the quantum confinement effect in the Si QD. The PL spectra of B-Si QDs and R-Si QDs samples show maximum peak energy at 410 nm (3.02 eV) and 700 nm (1.77 eV), respectively, while the quantum yield of Si QDs decreases from 5.8 to 34.6% when the average size decreases from 2.5 to 5.1 nm. The above results of PL emission spectroscopy and UV-vis absorption show quantum confined effect in Si QD.

Data Availability

The data used to support the findings of this study are included within the article.

Conflicts of Interest

The authors declare that they have no conflicts of interest.

Acknowledgments

This research was supported by the researcher program of Thuyloi University, Vietnam (TLU.STF.19–07).

References

[1] P. V. Kamat, "Quantum dot solar cells. Semiconductor nanocrystals as light harvesters," *The Journal of Physical Chemistry C*, vol. 112, no. 48, pp. 18737–18753, 2008.

[2] A. D. Dukes 3rd., P. C. Samson, J. D. Keene, L. M. Davis, J. P. Wikswo, and S. J. Rosenthal, "Single-nanocrystal spectroscopy of white-light-emitting CdSe nanocrystals," *The Journal of Physical Chemistry A*, vol. 115, no. 16, pp. 4076–4081, 2011.

[3] F. Peng, Y. Su, Y. Zhong, C. Fan, S.-T. Lee, and Y. He, "Silicon nanomaterials platform for bioimaging, biosensing, and cancer therapy," *Accounts of Chemical Research*, vol. 47, no. 2, pp. 612–623, 2014.

[4] H. Zhao, G. Liu, S. You et al., "Gram-scale synthesis of carbon quantum dots with a large Stokes shift for the fabrication of eco-friendly and high-efficiency luminescent solar concentrators," *Energy & Environmental Science*, vol. 14, no. 1, pp. 396–406, 2021.

[5] T.-H. Le and H.-D. Jeong, "The effects of electronic coupling between capping molecules and quantum dots on the light absorption and emission of octyl, styryl, and 4-ethynylstyryl terminated silicon quantum dots," *Physical Chemistry Chemical Physics*, vol. 16, no. 35, pp. 18821–18826, 2014.

[6] R. K. Baldwin, K. A. Pettigrew, E. Ratai, M. P. Augustine, and S. M. Kauzlarich, "Solution reduction synthesis of surface stabilized silicon nanoparticles," *Chemical Communications*, vol. 8, no. 17, pp. 1822-1823, 2002.

[7] J. G. C. Veinot, "Synthesis, surface functionalization, and properties of freestanding silicon nanocrystals," *Chemical Communications*, vol. 38, no. 40, pp. 4160–4168, 2006.

[8] C. M. Hessel, E. J. Henderson, and J. G. C. Veinot, "An Investigation of the formation and growth of oxide-embedded silicon nanocrystals in hydrogen silsesquioxane-derived nanocomposites," *The Journal of Physical Chemistry C*, vol. 111, no. 19, pp. 6956–6961, 2007.

[9] M. Dasog and J. G. C. Veinot, "Solid-state synthesis of luminescent silicon nitride nanocrystals," *Chemical Communications*, vol. 48, no. 31, pp. 3760–3762, 2012.

[10] A. Meldrum, R. F. J. Haglund, L. A. Boatner, and C. W. White, "Nanocomposite materials formed by ion implantation," *Advanced Materials*, vol. 13, no. 19, pp. 1431–1444, 2001.

[11] M. Zacharias, J. Heitmann, R. Scholz, U. Kahler, M. Schmidt, and J. Bläsing, "Size-controlled highly luminescent silicon nanocrystals: a SiO/SiO_2 superlattice approach," *Applied Physics Letters*, vol. 80, no. 4, p. 661, 2002.

[12] T.-H. Le and H.-D. Jeong, "Synthesis of silicon nanocrystal by magnesium directed reduction of the silica nanoparticle formed in micro-emulsion of reverse micelle," *Bulletin of the Korean Chemical Society*, vol. 35, no. 12, pp. 3421-3422, 2014.

[13] H. Yoo and J. Pak, "Synthesis of highly fluorescent silica nanoparticles in a reverse microemulsion through double-layered doping of organic fluorophores," *Journal of Nanoparticle Research*, vol. 15, p. 1609, 2013.

[14] S. Sankar, S. K. Sharma, N. Kaur et al., "Biogenerated silica nanoparticles synthesized from sticky, red, and brown rice husk ashes by a chemical method," *Ceramics International*, vol. 42, no. 4, pp. 4875–4885, 2016.

[15] Z. Favors, W. Wang, H. H. Bay et al., "Scalable synthesis of nano-silicon from beach sand for long cycle life Li-ion batteries," *Scientific Reports*, vol. 4, p. 5623.

[16] K. Sato, H. Tsuji, K. Hirakuri, N. Fukata, and Y. Yamauchi, "Controlled chemical etching for silicon nanocrystals with wavelength-tunable photoluminescence," *Chemical Communications*, vol. 25, no. 25, pp. 3759–4376, 2009.

[17] C.-S. Yang, R. A. Bley, S. M. Kauzlarich, H. W. H. Lee, and G. R. Delgado, "Synthesis of alkyl-terminated silicon nanoclusters by a solution route," *Journal of the American Chemical Society*, vol. 121, no. 22, pp. 5191–5195, 1999.

[18] M. X. Dung, D. D. Tung, S. Jeong, and H.-D. Jeong, "Tuning optical properties of Si quantum dots by π-conjugated capping molecules," *Chemistry-An Asian Journal*, vol. 8, no. 3, pp. 653–664, 2013.

[19] Y. Yu, G. Fan, A. Fermi et al., "Size-dependent photoluminescence efficiency of silicon nanocrystal quantum dots," *The Journal of Physical Chemistry C*, vol. 121, no. 41, pp. 23240–23248, 2017.

[20] X. Liu, Y. Zhang, T. Yu et al., "Optimum quantum yield of the light emission from 2 to 10 nm hydrosilylated silicon quantum dots," *Particle & Particle Systems Characterization*, vol. 33, no. 1, pp. 44–52, 2016.

[21] M. Dasog, Z. Yang, S. Regli et al., "Chemical insight into the origin of red and blue photoluminescence arising from freestanding silicon nanocrystals," *ACS Nano*, vol. 7, no. 3, pp. 2676–2685, 2013.

[22] J. Fuzell, A. Thibert, T. M. Atkins et al., "Red states versus blue states in colloidal silicon nanocrystals: exciton sequestration into low-density traps," *The Journal of Physical Chemistry Letters*, vol. 4, no. 21, pp. 3806–3812, 2013.

[23] A. M. Brouwer, "Standards for photoluminescence quantum yield measurements in solution (IUPAC technical report)," *Pure and Applied Chemistry*, vol. 83, no. 12, pp. 2213–2228, 2011.

[24] M. L. Mastronardi, F. Maier-Flaig, D. Faulkner et al., "Size-dependent absolute quantum yields for size-separated colloidally-stable silicon nanocrystals," *Nano Letters*, vol. 12, no. 1, pp. 337–342, 2012.

[25] R. Q. Zhang, A. D. Sarkar, T. A. Niehaus, and T. Frauenheim, "Excited state properties of Si quantum dots," *Physica Status Solidi B*, vol. 249, no. 2, pp. 401–412, 2012.

[26] L. Pavesi and R. Turan, *Silicon Nanocrystals Fundamental, Synthesis and Applications*, John Wiley & Sons, Hoboken, NY, USA, 2010.

[27] A. Puzder, A. J. Williamson, J. C. Grossman, and G. Galli, "Computational studies of the optical emission of silicon nanocrystals," *Journal of the American Chemical Society*, vol. 125, no. 9, pp. 2786–2791, 2003.